Monthly Notices
of the
ROYAL ASTRONOMICAL SOCIETY

Mon. Not. R. Astron. Soc. **427,** 3230–3243 (2012) doi:10.1111/j.1365-2966.2012.22026.x

# Spectrophotometric investigation of Phobos with the *Rosetta* OSIRIS-NAC camera and implications for its collisional capture

M. Pajola,[1⋆] M. Lazzarin,[2] I. Bertini,[1] F. Marzari,[2] D. Turrini,[3] S. Magrin,[2] F. La Forgia,[2] N. Thomas,[4] M. Küppers,[5] R. Moissl,[5] F. Ferri,[1] C. Barbieri,[1,2] H. Rickman,[6,7] H. Sierks[8] and the OSIRIS Team†

[1]*Centre of Studies and Activities for Space 'G. Colombo', University of Padova, Via Venezia 15, 35131 Padova, Italy*
[2]*Department of Physics and Astronomy of the University of Padova, Via Marzolo 8, 35131 Padova, Italy*
[3]*Institute for Interplanetary Space Physics, INAF, Via del Fosso del Cavaliere 100, 00133 Rome, Italy*
[4]*Physikalisches Institut, Sidlerstr. 5, University of Bern, 3012 Bern, Switzerland*
[5]*European Space Agency – European Space Astronomy Centre, PO Box 78, 28691 Villanueva de la Cañada, Spain*
[6]*Department of Physics and Astronomy, Uppsala University, Box 516, SE-75120 Uppsala, Sweden*
[7]*PAS Space Research Center, Bartycka 18A, PL-00-716 Warszawa, Poland*
[8]*Max-Planck-Institut für Sonnensystemforschung, Max-Planck-Strasse 2, 37191 Katlenburg-Lindau, Germany*

Accepted 2012 August 31. Received 2012 August 24; in original form 2012 March 16

**ABSTRACT**

The Martian satellite Phobos has been observed on 2007 February 24 and 25, during the pre- and post-Mars closest approach (CA) of the ESA *Rosetta* spacecraft Mars swing-by. The goal of the observations was the determination of the surface composition of different areas of Phobos, in order to obtain new clues regarding its nature and origin. Near-ultraviolet, visible and near-infrared (263.5–992.0 nm) images of Phobos's surface were acquired using the Narrow Angle Camera of the OSIRIS instrument onboard *Rosetta*. The six multi-wavelength sets of observations allowed a spectrophotometric characterization of different areas of the satellite, belonging respectively to the leading and trailing hemisphere of the anti-Mars hemisphere, and also of a section of its sub-Mars hemisphere. The pre-CA spectrophotometric data obtained with a phase angle of 19° have a spectral trend consistent within the error bars with those of unresolved/disc-integrated measurements present in the literature. In addition, we detect an absorption band centred at 950 nm, which is consistent with the presence of pyroxene. The post-CA observations cover from NUV to NIR a portion of the surface (0° to 43°E of longitude) never studied before. The reflectance measured on our data does not fit with the previous spectrophotometry above 650 nm. This difference can be due to two reasons. First, the OSIRIS observed area in this observation phase is completely different with respect to the other local specific spectra and hence the spectrum may be different. Secondly, due to the totally different observation geometry (the phase angle ranges from 137° to 140°), the differences of spectral slope can be due to phase reddening. The comparison of our reflectance spectra, both pre- and post-CA, with those of D-type asteroids shows that the spectra of Phobos are all redder than the mean D-type spectrum, but within the spectral dispersion of other D-types. To complement this result, we performed an investigation of the conditions needed to collisionally capture Phobos in a way similar to that proposed for the irregular satellites of the giant planets. Once put in the context of the current understanding of the evolution of the early Solar system, the coupled observational and dynamical results we obtained strongly argue for an early capture of Phobos, likely immediately after the formation of Mars.

**Key words:** techniques: imaging spectroscopy – planets and satellites: formation – planets and satellites: individual: Phobos – planets and satellites: surfaces.

⋆E-mail: maurizio.pajola@studenti.unipd.it, maurizio.pajola@gmail.com
†M. A'Hearn, F. Angrilli, A. Barucci, J.-L. Bertaux, G. Cremonese, B. Davidsson, V. Da Deppo, S. Debei, M. De Cecco, S. Fornasier, M. Fulle, O. Groussin, P. Gutierrez, S. Hviid, W.-H. Ip, L. Jorda, H. U. Keller, J. Knollenberg, D. Koschny, J. R. Kramm, E. Kuehrt, P. Lamy, L. M. Lara, J. J. Lopez-Moreno, H. Michalik, G. Naletto, R. Rodrigo, L. Sabau, K.-P. Wenzel.

## 1 INTRODUCTION

The inner Martian satellite Phobos has been the subject of several photometric and spectroscopic studies ranging from the near-ultraviolet (NUV) to the near-infrared (NIR) over the past 40 years.

The first photometric observation was performed by the NASA *Mariner* 9 spacecraft which led to a disc-integrated analysis of the leading hemisphere of Phobos. The NASA *Viking Lander II* camera then observed a disc-integrated sub-Mars hemisphere. All these observations indicated a dark and flat visible spectrum which was considered consistent with a carbonaceous chondrite composition (Masursky et al. 1972; Pollack et al. 1978; Pang et al. 1980).

In 1989 the photometric disc-resolved observation of Phobos by the Videospectrometric Camera (VSK), the Combined Radiometer and Photometer for Mars (KRFM) and the Imaging Spectrometer for Mars (ISM) onboard the USSR *Phobos 2* spacecraft observed leading and trailing parts of the anti-Mars hemisphere and part of the sub-Mars hemisphere. Thanks to the possibility of investigating the spectral behaviour of specific and resolved areas, Phobos could be divided into different geological units, characterized by different colour and morphology. The fresher areas associated with the Stickney crater, i.e. the leading hemisphere of Phobos, were found to be bluer in colour than the background areas of the redder trailing hemisphere (Murchie & Erard 1996).

Later disc-integrated observations of the leading hemisphere of Phobos were performed by the *Hubble Space Telescope* Faint Object Spectrograph (*HST*-FOS). FOS and VSK/KRFM/ISM observations yielded significantly redder spectra than previous spectrophotometric observations (Zellner & Wells 1994; Murchie & Erard 1996).

Disc-integrated analysis of the *HST* Wide-Field Planetary Camera 2 (WFPC2) data had shown a weak spectral absorption feature between 953 and 1042 nm, indicating the possible existence of pyroxene on the surface (Cantor et al. 1999). However, different types of meteorites gave no conclusive analogues to the surface reflectance spectrum (Cantor et al. 1999).

After the arrival of the NASA *Mars Pathfinder* in 1997, a set of sub-Mars disc-integrated observations were realized through the use of the Imager for *Mars Pathfinder* (IMP). In this work the redder spectra seen by FOS and VSK/KRFM/ISM were confirmed (Thomas et al. 1999) and it was indicated that the spectral slope of Phobos is comparable to D-type reference asteroids (Murchie 1999).

In 1999 and in 2003, Phobos was observed with the NASA Infrared Telescope Facility on Mauna Kea, Hawaii. The first IR observations regarded the entire surface of Phobos and it was confirmed that the leading (Stickney-dominated) and the trailing sides of Phobos were best matched by T-type and D-type asteroids, respectively (Rivkin et al. 2002). The following 2003 Phobos IR observations showed that the acquired spectra were consistent with those of Murchie (1999) and Rivkin et al. (2002) but with better spectral resolution (Lynch et al. 2007).

Close encounters of the ESA *Mars Express* (*MEX*) spacecraft with Phobos happened in 2004. A UV spatially resolved observation of a sub-Mars hemisphere part of Phobos was performed, using the Ultraviolet and Infrared Atmospheric Spectrometer (SPICAM) instrument. Similarly, the Observatoire pour la Mineralogie, l'Eau, les Glaces et l'Activité instrument (OMEGA) onboard *MEX* acquired hyperspectral data of resolved areas located north-east of the Stickney crater. Resolved and specifically located areas on the surface of Phobos indicated different spectral slopes with respect to those obtained by VSK, KRFM and ISM, this depending on different selected locations with respect to those observed by *Phobos 2* instruments (Perrier, Stern & Bertaux 2004; Gondet et al. 2008, 2009; Gondet, Bibring & Langevin 2010).

On 2007 October 23 the Compact Reconnaissance Imaging Spectrometer for Mars (CRISM) onboard the NASA *Mars Reconnaissance Orbiter* acquired disc-resolved data of the same area observed by the OMEGA instrument three years before, indicating, as well, spatial variations in spectral slopes with respect to *Phobos 2* instruments (Murchie et al. 2007, 2008).

On 2007 February 24 and 25, the Optical, Spectroscopic and Infrared Remote Imaging System Narrow Angle Camera (OSIRIS-NAC) instrument onboard the ESA *Rosetta* spacecraft observed Phobos from the near-UV to the near-IR. These observations led to a disc-integrated spectrophotometric analysis of different surface areas of the satellite which is going to be presented in the following sections.

In this paper the *Rosetta* fly-by geometry will be presented together with the OSIRIS Phobos observation set. The data analysis regarding pre- and post-Mars closest approach (CA) is then illustrated, giving particular emphasis to the spectrophotometric studies performed on the multispectral resolved area longitude range from 0° to 43°E, which has not been studied before. A final part is then dedicated to the nature of Phobos and its possible asteroidal collisional capture origin.

## 2 THE *ROSETTA* FLY-BY GEOMETRY

On 2007 February 24 and 25, the *Rosetta* spacecraft flew by the planet Mars. This was one of the four gravity assists (three Earth swing-bys performed on 2004 March 4, 2007 November 13 and 2009 November 13, respectively, and one Mars fly-by) foreseen during its complex interplanetary trajectory towards its main target, comet 67P/Churyumov–Gerasimenko.

The gravitational assist geometry of the *Rosetta*/Mars swing-by provided an opportunity to study Phobos during the pre- and post-Mars CA, from distances which varied from 115 000 to 21 000 km. The *Rosetta* spacecraft attitude allowed two visibility times with Phobos inside the NAC field of view which are presented in Table 1, while NAC-specific observation time ranges are indicated in Table 2.

In Fig. 1 a sketch of the trajectories of *Rosetta* and the Martian satellites during the fly-by is shown.

## 3 OBSERVATION SETS

In the following, specific previous works regarding studies of Phobos are presented; in this context the OSIRIS-NAC observations are inserted.

### 3.1 Previous works

The Phobos surface areas covered by all previous NUV, visible and NIR unresolved or resolved observations from *Mariner 9* to *Mars Express* are presented in Figs 2 and 3 where they are over-plotted on the USGS *Viking* Phobos map, together with the small bodies latitude and longitude grid, the trailing and the leading hemispheres

**Table 1.** Phobos visibility times inside the NAC field of view for the entire *Rosetta*/Mars swing-by.

| Date | Visibility UT times |
|---|---|
| 2007 Feb 24 | 22:05:58.283–22:18:07.004 |
| 2007 Feb 25 | 02:31:31.569–02:59:59.984 |

**Table 2.** OSIRIS-NAC sets obtained between 2007 February 24 and 25. The set number, the acquisition date, the observation time intervals, the spacecraft–Phobos distance ranges and the respective scales are presented together with the image dimensions and the number of images acquired.

| Set no. | Date | Observation time UT | Distance range (km) | Scale range (m pixel$^{-1}$) | Dimensions (pixel) | Number of images |
|---|---|---|---|---|---|---|
| 1 | 2007 Feb 24 | 22:09:09.707–22:10:04.149 | 114 882–114 467 | 2166–2158 | 2048 × 2048 | 11 |
| 2 | 2007 Feb 25 | 02:39:11.416–02:39:36.884 | 20 786–21 057 | 391–397 | 256 × 256 | 12 |
| 3 | 2007 Feb 25 | 02:41:12.425–02:41:37.743 | 22 079–22 350 | 416–421 | 256 × 256 | 12 |
| 4 | 2007 Feb 25 | 02:43:12.425–02:43:37.738 | 23 365–23 636 | 440–445 | 256 × 256 | 12 |
| 5 | 2007 Feb 25 | 02:45:12.427–02:45:37.703 | 24 654–24 926 | 464–469 | 256 × 256 | 11 |
| 6 | 2007 Feb 25 | 02:47:12.427–02:47.37.770 | 25 946–26 219 | 489–492 | 256 × 256 | 12 |

of the satellite, and the anti-Mars and sub-Mars hemispheres of Phobos.

In Fig. 2 the sub-*HST* latitude and longitude point ranges of WFPC2 are indicated. The *HST*-WFPC2 observations were acquired in the 10.°6–40.°5 phase angle range and led to a disc-integrated analysis (Cantor et al. 1999). In Fig. 2 the sub-*Mars Pathfinder* latitude and longitude points of IMP are also indicated. These observations regarded three pixels across Phobos and led to a disc-integrated analysis. The IMP observation of 1997 August 30 was performed with a phase angle of 28°, while the 1997 September 12 observation was realized at a phase angle of 54° (Thomas et al. 1999). *Mariner* 9 data allowed a disc-integrated analysis of Phobos's leading hemisphere (Masursky et al. 1972; Pang et al. 1980). *Viking Lander II* observations regarded a disc-integrated sub-Mars hemisphere and the spectral behaviour of Phobos's surface has been extrapolated as if the satellite had been observed at 0° phase angle (Pollack et al. 1978). The *HST* FOS observations led again to a disc-integrated analysis of the leading hemisphere of Phobos (Zellner & Wells 1994).

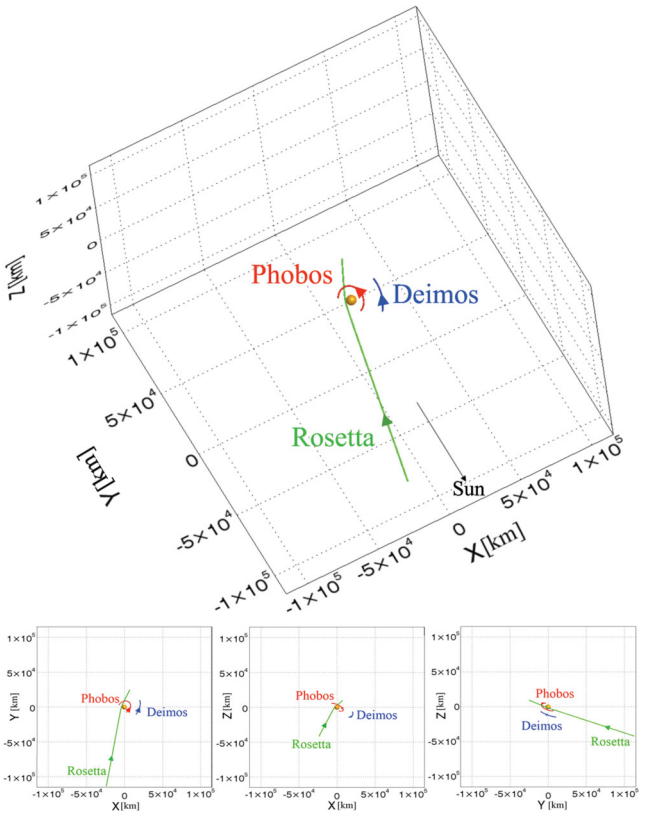


**Figure 1.** *Rosetta* (green), Phobos (red) and Deimos (blue) ecliptic orbits between 22:09 and 02:47 UT, together with their *XY*, *XZ* and *YZ* plane projections in a Mars centred reference frame referred to equinox J2000. The orbit directions are indicated with an arrow-head. The direction of the Sun is also indicated with a black arrow in the upper image. The *Rosetta* closest approach to Mars was on 2007 February 25 at 01:54 UT with an altitude of 250 km from the planet's surface.

Fig. 3 shows the resolved observations performed from a distance of several hundred kilometres by the VSK camera with a scale of 260–570 m pixel$^{-1}$, the KRFM spectrometer with a FOV of 1 km$^2$ on the surface of Phobos and the ISM imaging spectrometer with a scale of 700 m pixel$^{-1}$, all co-aligned and with a phase angle of 7.°7 (Murchie & Erard 1996). OMEGA observation locations and the SPICAM observed area are also presented in Fig. 3, the first being performed from a distance of 149 km with a corresponding scale of 170 m pixel$^{-1}$ and a phase angle of 62.°6 (Gondet et al. 2008, 2009, 2010), and the latter being obtained at 162 km, a band resolution of 500 m and a phase angle of 61.°5 (Perrier et al. 2004).

### 3.2 OSIRIS-NAC observations

The observations used in this work are presented in Table 2.

The images have been divided into two groups, the pre- and the post-Mars CA phases respectively. Both are presented in Table 2. The sub-*Rosetta* latitude and longitude points, the sub-solar latitude and longitude points and the phase angle for each observation set are presented in Table 3.

The bandpass filters which have been used in the pre- and post-Mars CA are indicated in Table 4. We underline that the filter set used is optimized for studying the chemical and physical structure of the comet 67P/Churyumov–Gerasimenko nucleus, this comet being the main *Rosetta* target; the use of these filters is also suitable for studying the surface chemical composition of Phobos. A description of each NAC filter is presented in Keller et al. (2007).

The OSIRIS-NAC first set was obtained on 2007 February 24 between 22:09:09 and 22:10:04 UT. Although the distance range in this time interval varied by 415 km, due to the *Rosetta* velocity of 9.3 km s$^{-1}$, the scale changes only by 8 m pixel$^{-1}$. This means that all the images acquired in this range can be considered at the same scale. In the post-Mars CA phase five sets have been obtained, while the *Rosetta* space probe was leaving Mars with a velocity of 10.9 km s$^{-1}$. In each set the distance varies by 271 km, but the scale changes only by 5 m pixel$^{-1}$.

All images belonging to the same set are treated as if they were taken at the same distance and the same scale.

As can be seen in Table 3, all phase angles inside a single observation set, independently from the pre- or post-Mars CA, present negligible variations from 0.°06 to 0.°17. This allows us to consider the phase angle as constant in each set throughout the whole

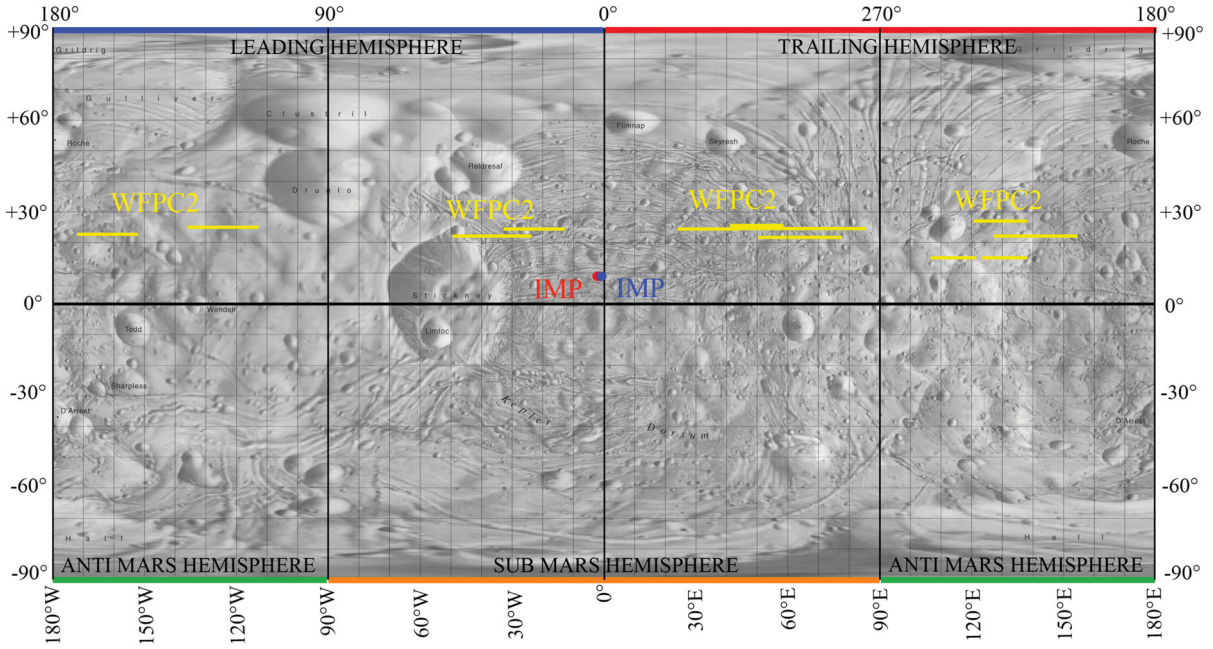


**Figure 2.** *Viking* Phobos map. The unresolved observation location ranges performed with *HST*-WFPC2 are overlapped with yellow lines, which represent the sub-*HST* latitude/longitude point range values of the disc-integrated analysis; the red and the blue dots are the sub-IMP latitude/longitude points on 1997 August 30 and September, respectively. Map credit: USGS/Peter Thomas/Phil Stooke. Scientific processing and annotation carried out by the author (MP) on the original USGS image.

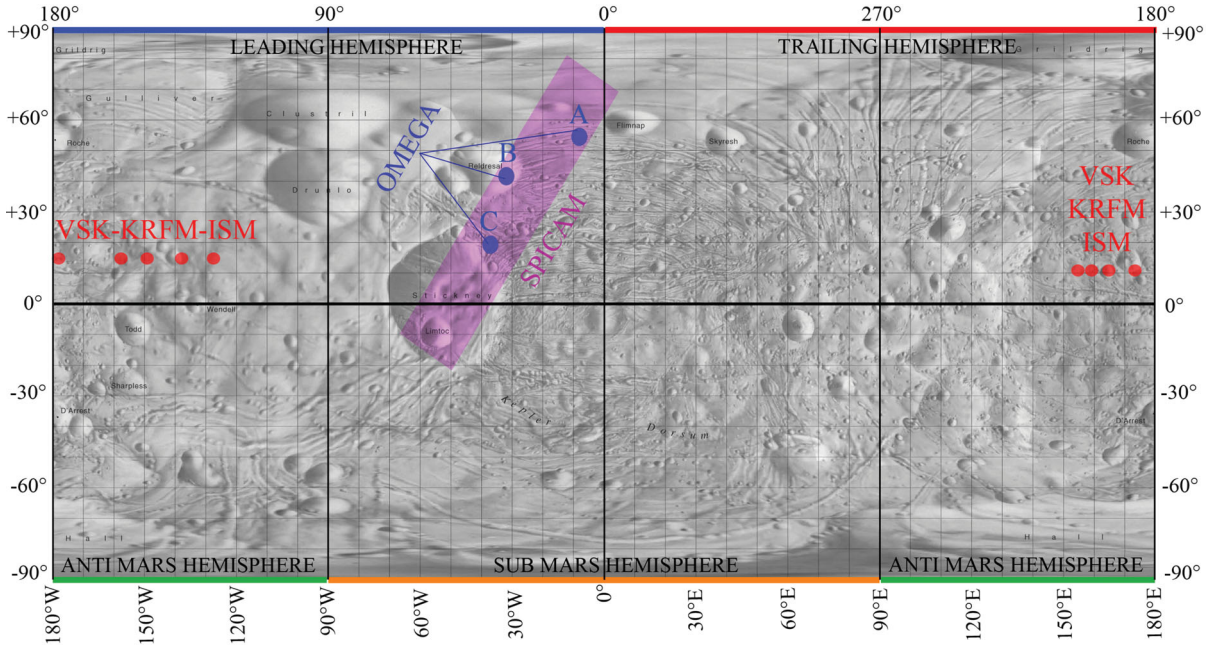


**Figure 3.** *Viking* Phobos map. The resolved observation locations performed with VSK, KRFM and ISM are overlapped with red dots; OMEGA observation locations are overlapped with blue dots on the three (A, B, C) areas observed; and SPICAM observations were performed on the violet rectangular area. Map credit: USGS/Peter Thomas/Phil Stooke. Scientific processing and annotation carried out by the author (MP) on the original USGS image.

observational range. The same consideration can be inferred also with the sub-*Rosetta* latitude/longitude point and also the sub-solar latitude/longitude point. The Phobos OSIRIS images sequence is presented in Fig. 4, where the first image for each set, obtained with the F82–F22 filter combination, is shown, together with the set number indicated in Table 2.

The Phobos surface areas observed on 2007 February 24 and 25 with NAC at 22:09:09 and 02:39:11 UT, respectively, are presented in Fig. 5; the green area is the observed side in the pre-Mars CA set 1, while the yellow area is the resulting surface of Phobos observed in set 2 during post-Mars CA.

Two false-colour images of the pre-Mars CA observation set 1 are presented in Figs 6 and 7, showing the equatorial view of the Mars–Phobos system as observed by OSIRIS. Fig. 7 is a false-colour image centred in the blue–NUV part of the electromagnetic spectrum. This is the first resolved image of Phobos in this wavelength range.

**Table 3.** OSIRIS Phobos dedicated sets obtained during Mars swing-by. The table gives the ranges of the sub-*Rosetta* latitude and longitude points, of the sub-solar latitude and longitude points, and of the computed phase angles. The filters used in all sets are presented in Table 4.

| Set no. | Sub-*Rosetta* latitude range | Sub-*Rosetta* longitude range | Sub-solar latitude range | Sub-solar longitude range | Phase angle (°) |
|---|---|---|---|---|---|
| 1 | −0.05 to −0.04 | 146.62 E to 145.85 E | −3.21 to −3.21 | 165.24 E to 164.53 E | 18.89 to 18.95 |
| 2 | −2.13 to −2.20 | 90.65 E to 90.49 E | −3.26 to −3.26 | 46.47 W to 46.81 W | 136.80 to 136.97 |
| 3 | −2.45 to −2.51 | 89.87 E to 89.70 E | −3.26 to −3.26 | 48.07 W to 48.40 W | 137.58 to 137.73 |
| 4 | −2.73 to −2.78 | 89.03 E to 88.84 E | −3.26 to −3.26 | 49.66 W to 49.99 W | 138.27 to 138.41 |
| 5 | −2.98 to −3.03 | 88.12 E to 87.92 E | −3.26 to −3.26 | 51.24 W to 51.58 W | 138.91 to 139.04 |
| 6 | −3.20 to −3.25 | 87.16 E to 86.96 E | −3.26 to −3.26 | 52.83 W to 53.16 W | 139.50 to 139.62 |

**Table 4.** NAC number, name, central wavelength and the full width to half-maximum (FWHM) of the filters used during the pre- and the post-Mars CA for the observation of Phobos.

| ID no. | Filter name | Wavelength (nm) | FWHM (nm) | Observation phase |
|---|---|---|---|---|
| F15 | FFP-UV Far-UV | 263.5 | 45.0 | Pre & post |
| F16 | FFP-UV Near-UV | 360.0 | 50.0 | Pre & post |
| F84 | Neutral Blue | 480.0 | 72.0 | Pre |
| F24 | FFP-Vis Blue | 480.5 | 73.0 | Post |
| F83 | Neutral Green | 535.0 | 60.0 | Pre |
| F23 | FFP-Vis Green | 535.5 | 61.0 | Post |
| F22 | FFP-Vis Orange | 648.5 | 83.0 | Post |
| F82 | Neutral Orange | 650.5 | 81.0 | Pre |
| F87 | Neutral Hydra | 700.5 | 21.0 | Pre |
| F27 | FFP-Vis Hydra | 700.5 | 21.0 | Post |
| F88 | Neutral Red | 742.5 | 61.0 | Pre |
| F28 | FFP-Vis Red | 743.0 | 62.0 | Post |
| F58 | Ortho_Red | 790.5 | 23.0 | Post |
| F51 | Ortho FFP-IR | 804.5 | 39.0 | Pre & post |
| F41 | Near-IR FFP-IR | 882.5 | 65.0 | Pre & post |
| F61 | $Fe_2O_3$ FFP-IR | 932.0 | 40.0 | Pre & post |
| F71 | IR FFP-IR | 992.0 | 44.0 | Pre & post |

## 4 DATA ANALYSIS

### 4.1 Pre-Mars CA observation

#### *4.1.1 Image set description*

The pre-Mars CA observation started at 22:09:09 UT and finished at 22:10:04 UT. In this time interval a set of 11 images of Phobos were obtained, revealing a resolved object. The images did not give the possibility of obtaining any feature of the surface due to the limited amount of sampling pixels (around 130 pixels), each with a scale of 2162 m pixel$^{-1}$. The observed area acquired in this set is presented in Fig. 5 where the observed surface is shown in green overlapped as a transparency on the *Viking* map. The area which we imaged during this phase coincides with the greater part of the Phobos anti-Mars hemisphere, but also a small section of the sub-Mars hemisphere is integrated. The total longitude range observed goes from 126°W to 286°W.

#### *4.1.2 Analysis methods*

We decided to perform a disc-integrated spectrophotometric analysis because of the low resolution.

The OSIRIS data were reduced using the calibration pipeline discussed by Magrin et al. (2012). The bias image has been subtracted from the raw data. The resulting image has been divided by the flat-field image and the background sky properly subtracted. Afterwards we measured the flux of Phobos and its error using the usual aperture photometry technique. We checked that no cosmic ray hit the detector. An inner radius of 10 pixels centred on the Phobos photocentre was used in order to contain all the light coming from the target. We considered an annulus between 19 and 21 pixels from the photocentre of the satellite in order to compute the flux of the sky background. We choose these values because in this range Phobos was close enough but no light from it fell inside.

Finally, we measured the reflectance of Phobos in the NUV–NIR range 200–1000 nm. In Fig. 8 we plot the resulting values obtained together with *Mariner* 9 spectrometer and *HST*-FOS data sets which both imaged the leading hemisphere of the satellite. We also plotted our result against *Viking Lander II* camera and IMP data sets, which both imaged the sub-Mars hemisphere and led to a disc-integrated analysis. The other two reference spectra were those obtained from *HST* WFPC2 on 1997 May 18 and on June 27, both are an example for the trailing and the leading hemisphere, studied with a disc-integrated analysis.

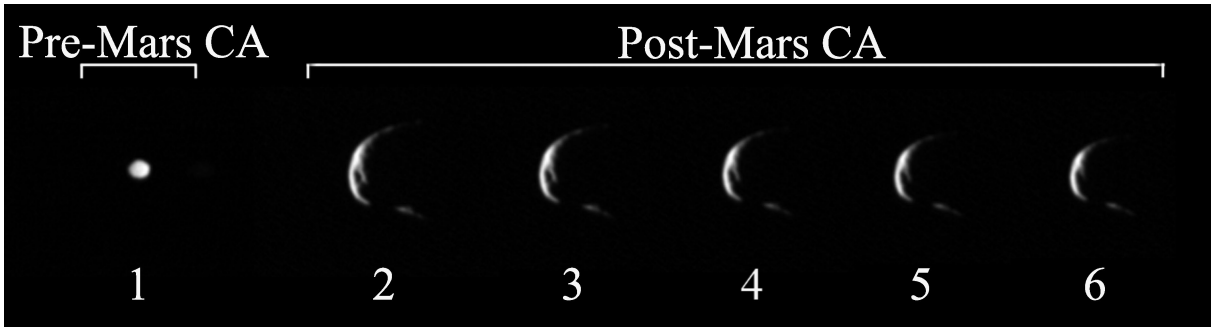


**Figure 4.** Mosaic view of the first image of each OSIRIS-NAC set obtained on 2007 February 24 and on 2007 February 25, respectively. The set numbers are those presented in Table 2.

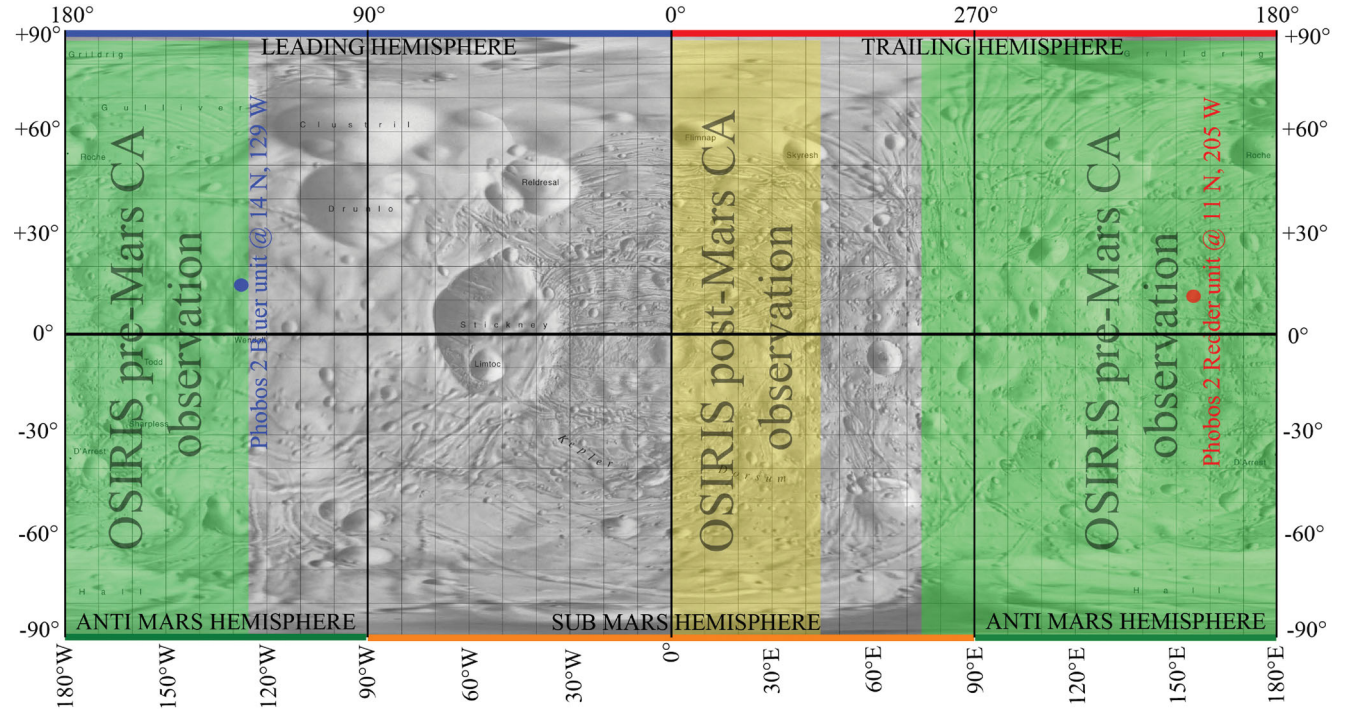


**Figure 5.** Images acquired on 2007 February 24 and 25 at 22:09:09 and 02:39:11 UT, respectively. The green area is the side observed in the pre-Mars CA set, while the yellow area is the surface observed in the first post-Mars CA set. All areas are over-plotted on the *Viking* map. Map credit: USGS/Peter Thomas/Phil Stooke. Scientific processing and annotation carried out by the author (MP) on the original USGS image.

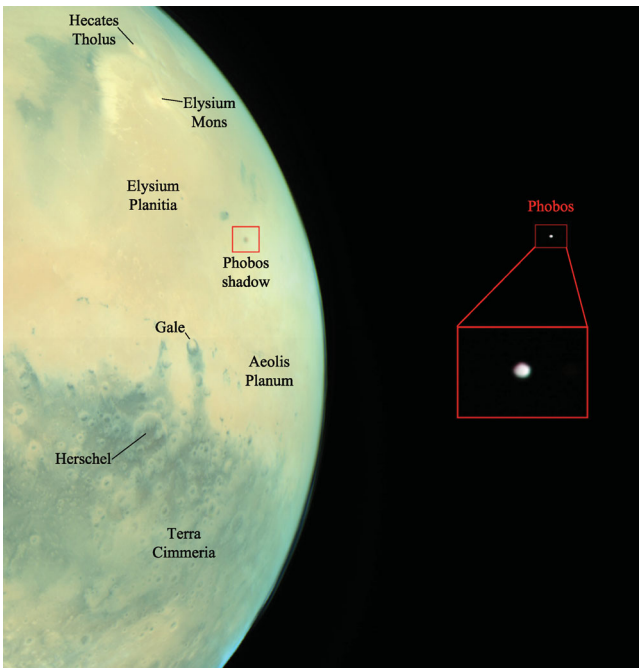


**Figure 6.** OSIRIS RGB image realized with filter F82 for the red channel, F83 for the green channel and F84 for the blue channel. The images were acquired at 22:09:09, 22:09:14 and 22:09:19 UT, respectively. Phobos is shown in the red boxes. The Phobos shadow position on the Martian surface is identified in the red square. Some Mars surface features are also identified and indicated as Hecates Tholus, Elysium Mons, Herschel, and Gale crater, the last one being the NASA *MSL-Curiosity* rover landing site.

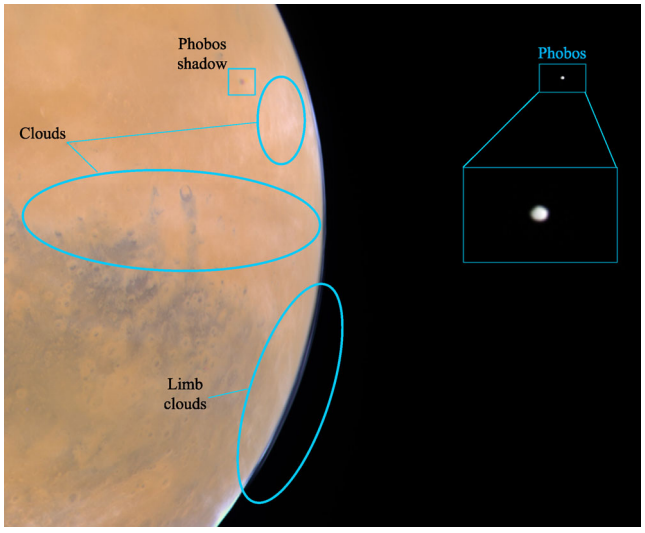


**Figure 7.** OSIRIS NUV false-colour image processed with filter F83 (red), F84 (green) and F16 (blue). The images were acquired at 22:09:19, 22:09:14 and 22:09:36 UT respectively. Phobos is shown in the light blue boxes. The Phobos shadow position on the Martian surface is recognizable in the blue square. In this blue–NUV triplet the Martian veils of clouds appear over the surface and at the planet limb.

### *4.1.3 Results and discussion*

All OSIRIS data fit within the errors[1] with spectral trends of previous measurements, except for those spectra obtained by *HST*-WFPC2 and the *Viking Lander II* camera.

[1] We underline that the error bars used in the spectrophotometric plot refer to the absolute flux calibration values, but the auto consistency of each image used for this analysis has been verified to be of the order of 1.5–2 per cent.

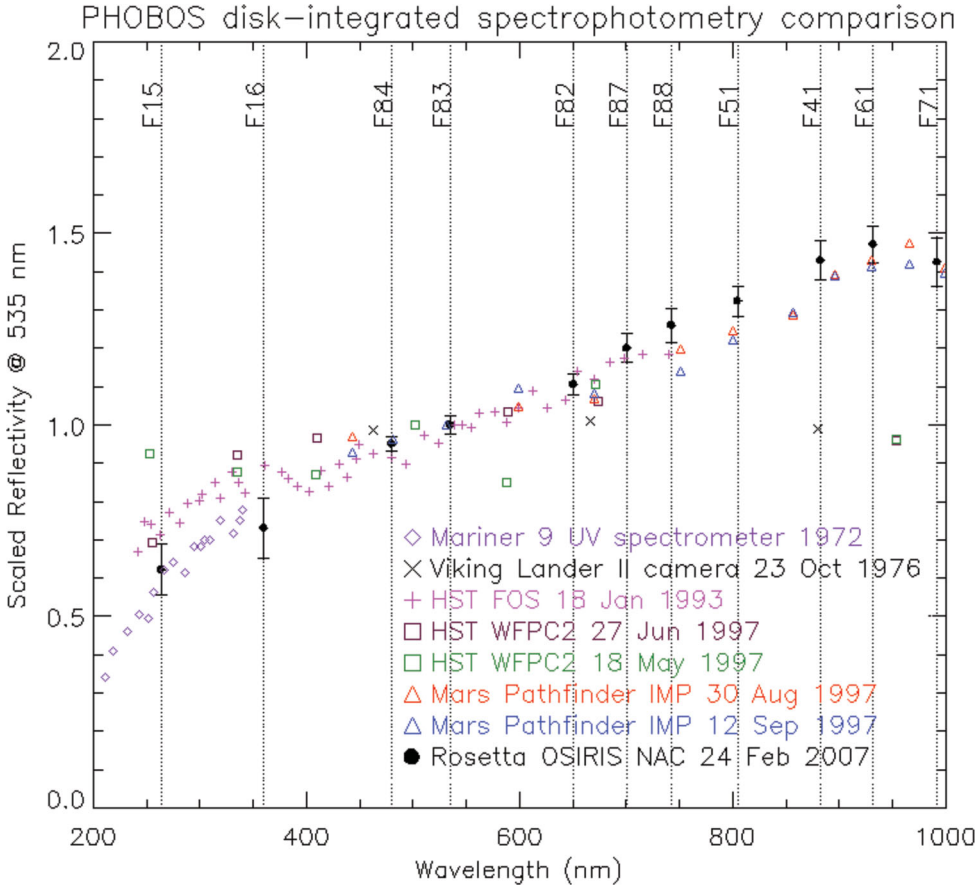


**Figure 8.** OSIRIS-NAC spectrum compared with previous spectrophotometric unresolved or disc-integrated observations.

The low points after 800 nm which belong to *HST*-WFPC2 and *Viking Lander* observations are more similar to the flat spectroscopic trend obtained by Pang et al. (1980) and Pollack et al. (1978) that indicated a mainly dark and flat visible spectrum instead of all following images obtained from the *Phobos 2* probe on. A possible explanation of these differences between bluer *HST*-WFPC2 and *Viking Lander* data with respect to all redder following data from the *Phobos 2* probe on could rely on different surface samplings between the bluer leading hemisphere/Stickney ejecta blanket with respect to the redder trailing hemisphere. The consequence of disc-integrated observations sampling a bigger area of the bluer leading hemisphere with respect to the total heterogeneous visible hemisphere could consequently be an explanation of this flatter spectral trend.

The OSIRIS data and all previous spectra used for comparison have been scaled to a reflectivity of 535 nm, except for *Mariner 9* data. The UV spectrometer data obtained from *Mariner 9* are centred in the NUV and there are no values that we could use in order to compute a factor that allowed scaling to 535 nm.

We decided not to plot in Fig. 8 the VSK/KRFM/ISM reflectance spectrum because it pertains to a specific unit located at 11°N, 205°W, and not to a disc-integrated analysis.

We also found in our data an interesting clue about the surface composition of Phobos which appears from NAC data. It is the 950 nm-centred band, which was already detected by Cantor et al. (1999). This spectral feature could be due to pyroxene, but since our longest wavelength data is at 992.0 nm we cannot confirm this feature because we had a poor sampling of its extent.

### 4.2 Post-Mars CA observation

#### *4.2.1 Image set description*

The *Rosetta*/Mars closest approach happened on 2007 February 25 at 01:54 UT, with an altitude of 250 km from the Martian surface. After the closest approach OSIRIS was redirected again towards Phobos, from 02:39:11 to 02:47.37 UT. The *Rosetta* orbit, together with the motion of the Martian satellites during this time interval, is presented in Fig. 9.

Five sets of multiband images were obtained through all available NAC filters (Table 4). The distance from the Martian satellite increased from 20 789 to 26 219 km, but gave the possibility to obtain resolved images, with resolution from 391 to 492 m pixel$^{-1}$. As shown in Fig. 10, the images obtained in this mission phase provide discernible surface features.

In Fig. 11 an image of the satellite, coloured in yellow, is superimposed on the *Viking* orthographic view centred at 270° of longitude. The resolved observed area of Phobos observed in the first post-Mars CA set is presented in Fig. 5 where the Phobos surface imaged is shown with yellow colour overlapped as a transparency on the *Viking* Phobos map. The most striking aspect of our observations during the post-Mars CA is that the sampled area has not been analysed before with multiband disc-resolved studies. Our results from this phase therefore extend the present knowledge of the surface composition of Phobos. The surface of Phobos which we observed goes from 0° to 43°E in longitude, entirely belonging to the sub-Mars hemisphere.

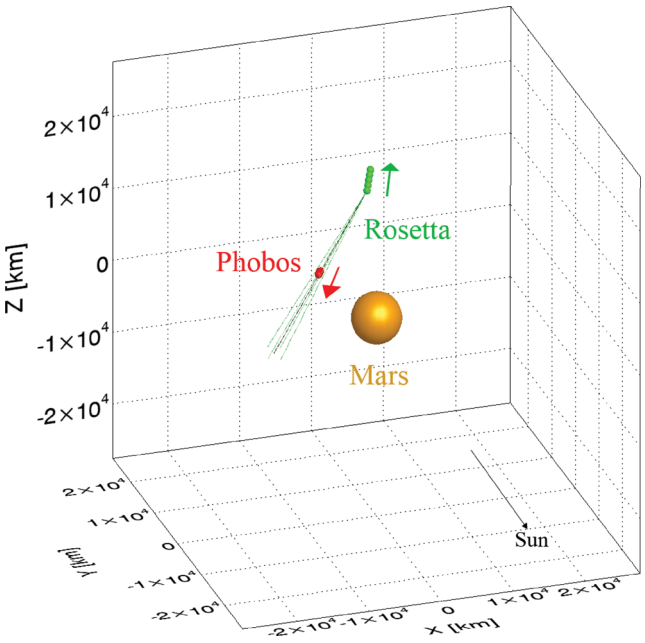


**Figure 9.** *Rosetta* post-Mars CA ecliptic orbit during NAC Phobos observation. Mars (orange), *Rosetta* (green) and Phobos (red) are indicated. Each of the five points of *Rosetta*, which is going further from the Mars or Phobos orbits, is the position at the time of acquisition of the first OSIRIS image of each set. The first acquired set at 02:39:11 UT presents also the NAC FOV with the four green lines departing from the spacecraft in the direction of Phobos; the OSIRIS NAC FOV centre is shown with the black line. The orbit steps in Fig. 9 are at 02:39:11, 02:41:12, 02:43:12, 02:45:12, 02:47:12 UT on 2007 February 25, respectively, and the orbit directions are indicated with arrows. The direction of the Sun is also indicated with a black arrow.

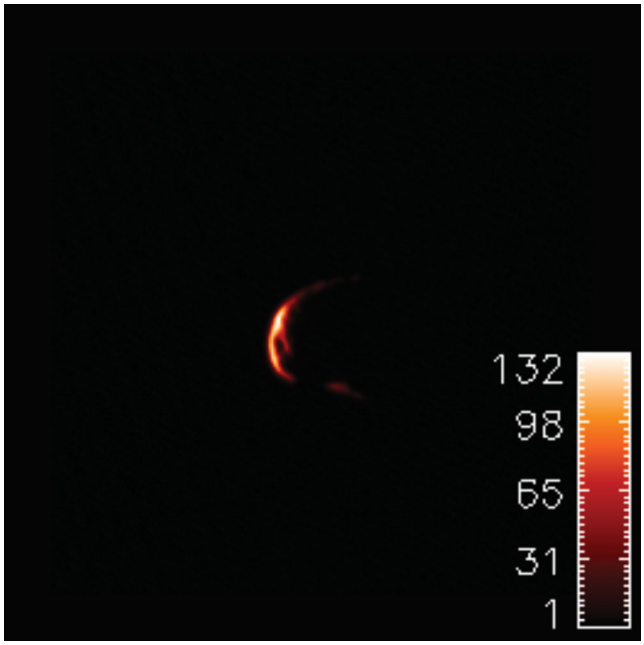


**Figure 10.** Phobos image, taken at 648.5 nm, as observed at 02:39:11 UT enhanced with a specific colourbar in order to better discern surface features. The colourbar values in the figure are in $10^{-5}$ W m$^{-2}$ sr$^{-1}$ nm$^{-1}$.

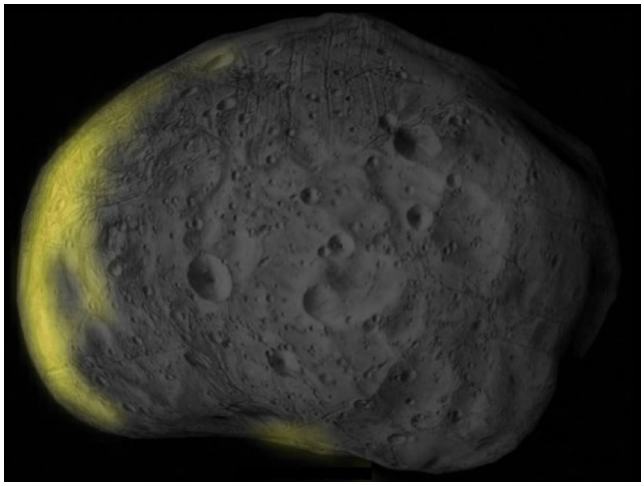

**Figure 11.** OSIRIS-NAC image (taken at 648.5 nm) of Phobos, whose crescent is the yellow part superimposed as a transparency on the *Viking* orthographic view centred at 270° of longitude. Scientific processing and annotation carried out by the author (MP) on the original image by A. Tayfun Oener/Calvin J. Hamilton.

In Fig. 12, the mutual conditions of geometry and observation between the Sun, Phobos and OSIRIS during this phase of the fly-by are reconstructed. Applying the same fly-by conditions of illumination on the Phobos Mercator-projection *Viking* altitude map, the shadowed equatorial area, close to the terminator, becomes discernible. The surrounding altitude values of this area are all 1.5 km higher than the centre of it, while the *Viking* values inside the dark area are the same: this is the reason why we consider this equatorial section an ancient crater with a central plain surrounded by illuminated peaks.

### *4.2.2 Analysis methods*

We analysed these data with the same techniques as applied to the pre-Mars CA phase.

The results of these studies have been plotted together with the spectra obtained from other spatially resolved studies, namely the VSK, KRFM and ISM reflectance spectrum obtained for the area belonging to the redder unit at 11°N, 205°W and for the area belonging to the bluer unit at 11°N, 129°W, and the *MEX* SPICAM spectrum obtained for the area presented in Fig. 3 together with areas A, B, C (indicated in Fig. 3) analysed by *MEX* OMEGA.

The data points obtained from the five NAC sets are plotted together in Fig. 13. All the data have been normalized at 535 nm, except for *MEX* SPICAM because there are no data close to 535 nm.

All NAC reflectance values agree with each other within the errors, showing that there are no significant variations between the five different sets, even if the phase angle changes from 137° to 140°. This is something to be expected considering the flat trend of the phase function for such observational angles of other airless Solar system bodies (Domingue et al. 2002; Lederer et al. 2008).

### *4.2.3 Results and discussion*

In Fig. 13 our data mostly do not fit with previously observed trends at wavelengths longer than 650 nm, showing a redder trend.

This can be due to two reasons. First, the OSIRIS observed area is completely different from the areas of the other specific spectra. As is the case for the OMEGA spectra, different areas were specifically selected close to Flimnap crater, area A (Gondet et al. 2008, 2009, 2010), inside Reldresal crater, area B, or close to Stickney crater, area C, all being completely in the bluer and trailing hemisphere of

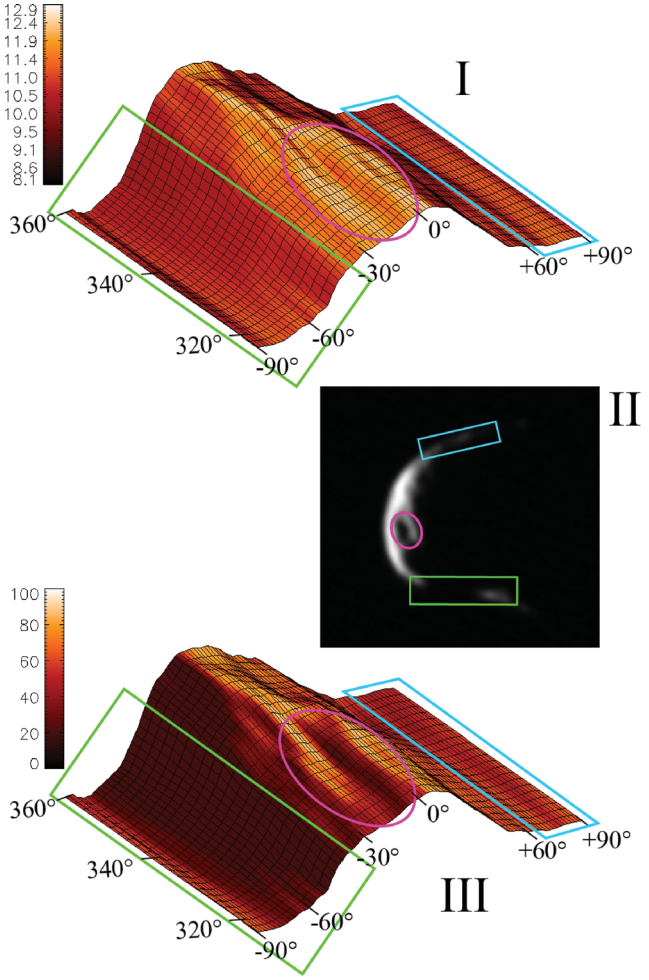


**Figure 12.** Panel I: Section of *Viking* altitude Mercator map of Phobos of the observed area imaged during the post-CA. The longitude spans from 316° to 360° while the latitude goes from the Phobos North to the Phobos South pole (+90° to −90°). The colourbar values in Panel I are in kilometres. Panel II: OSIRIS Phobos image. Panel III: percentage of illumination on the 3D *Viking* Mercator map of the Phobos (Panel I) observed area with the same illumination conditions during OSIRIS observation. The area selected in the pink ellipse refers to the half of the equatorial area where the visible crater is (dark shadowed plain surrounded by illuminated peaks). Looking at the pink ellipse in Panel III it is possible to see that the half of the equatorial area where the crater is located is illuminated with values that are less than 5 per cent, which means that there is shadow, which refers to the crater itself. The other half of the equatorial area in Panel III presents values of illumination bigger than 90 per cent, this corresponding to the left side of the crater of Phobos in Panel II. In the green rectangular area it is shown that from latitude −30° to −60° the entire observed surface of Phobos is in shadow (illumination values which are less than 5 per cent) while the South pole is illuminated with values bigger than 70 per cent, as can be seen with the OSIRIS image in Panel II. Looking at the OSIRIS image we can see that from the equator of Phobos to its North pole (light blue rectangular area) there is a constant diminution of the percentage of illumination along the crescent, which is also indicated in Panel III.

Phobos. *Phobos 2* VSK, KRFM, ISM reflectance spectra obtained at 14°N, 129°W coordinates differ from those data, even if they were obtained in the same hemisphere as the OMEGA observation; this is a possible consequence of the different specific area observed. OSIRIS data regard a section going from 0° to 43°E of the redder trailing hemisphere of Phobos, so these data are closer to the *Phobos 2* VSK, KRFM, ISM observations performed on an area located at 11°N, 205°W, but still do not fit with them. A possible reason is still the fact that the side we both observed is the reddest one but the areas analysed are different. This could indicate a possible heterogeneity of the surface of Phobos.

This has not been the case for the pre-Mars CA analysis, where the surface we observed with OSIRIS-NAC was already observed with different instruments and geometry, giving in fact a better fit inside the error bars with previous data.

The second possible explanation of the difference between OSIRIS data and *Phobos 2* redder unit data can be the strong difference of the observational geometry. NAC data were obtained with a phase angle which ranges from 137° to 140°, while *Phobos 2* data were obtained with a phase angle of 7°.7. Phase reddening, already observed on asteroids (Lumme & Bowell 1981) such as (433) Eros (Clark et al. 2002), (2867) Steins (Schröder, Lüthi & Gunderson 2009) and (21) Lutetia (Magrin et al. 2012), on the Moon (Buratti, Hillier & Wang 1996), and on Mercury (Warell & Bergfors 2008), could be invoked. The amount of phase reddening is dependent on the composition, but in the literature we can find values roughly of the order of 1–10 per cent at 100 nm from 0° to 150°.

The estimate of the spectral slope obtained between 360 and 992 nm from NAC pre-CA data is 10.2 per cent for 100 nm at 18°.9 of phase angle, while that from the post-CA data is 11.4 per cent for 100 nm at 138°.2 of phase angle. The phase reddening we obtained (about 1.2 per cent for 100 nm), if applied to *Phobos 2* data, is able to explain the difference between the redder spectrum of OSIRIS data and the *Phobos 2* data which present a spectral slope in the 360–990 nm range of 10.8 per cent for 100 nm at 7°.7 of phase angle.

## 5 CLUES ON THE ORIGIN OF PHOBOS

The origin of Phobos and the link between the composition of this Martian moon and its formation region are still a matter of debate, as recently reviewed by Rosenblatt (2011). In the following, we will address the possible scenario for the collisional capture of Phobos in light of the data supplied by OSIRIS suggesting a similarity with D-type asteroids, and discuss whether we can improve our understanding of the timing and the processes responsible for the capture.

The scenario we propose is dynamically more robust than the first capture model proposed by Hunten (1979), where an asteroid was driven into a planetocentric orbit around Mars by aerodynamic drag in a nebula surrounding the planet shortly after it formed. We instead show that it is possible to trap around Mars fragments of an impact between two asteroidal bodies occurring close to the Martian sphere of influence with a mechanism similar to that proposed for the origin of the irregular satellites of the outer planets (Colombo & Franklin 1971; Turrini, Marzari & Tosi 2009).

### 5.1 Surface composition of Phobos and its similarity to D-type asteroids

Assuming that the surface composition of Phobos can tell us about its origin, we compared our results with Bus mean D-type asteroid taxonomy (Bus & Binzel 2002a,b) and with some D-type reflectance spectra obtained by Lazzarin, Barbieri & Barucci (1995) and Bus & Binzel (2002a,b). We plotted as a comparison OSIRIS data obtained during the pre- and post-CA in the same wavelength range with the spectra of the D-type asteroids 336 Lacadiera, 1167 Dubiago and 2246 Bowell – see Fig. 14. We decided to plot these three spectra

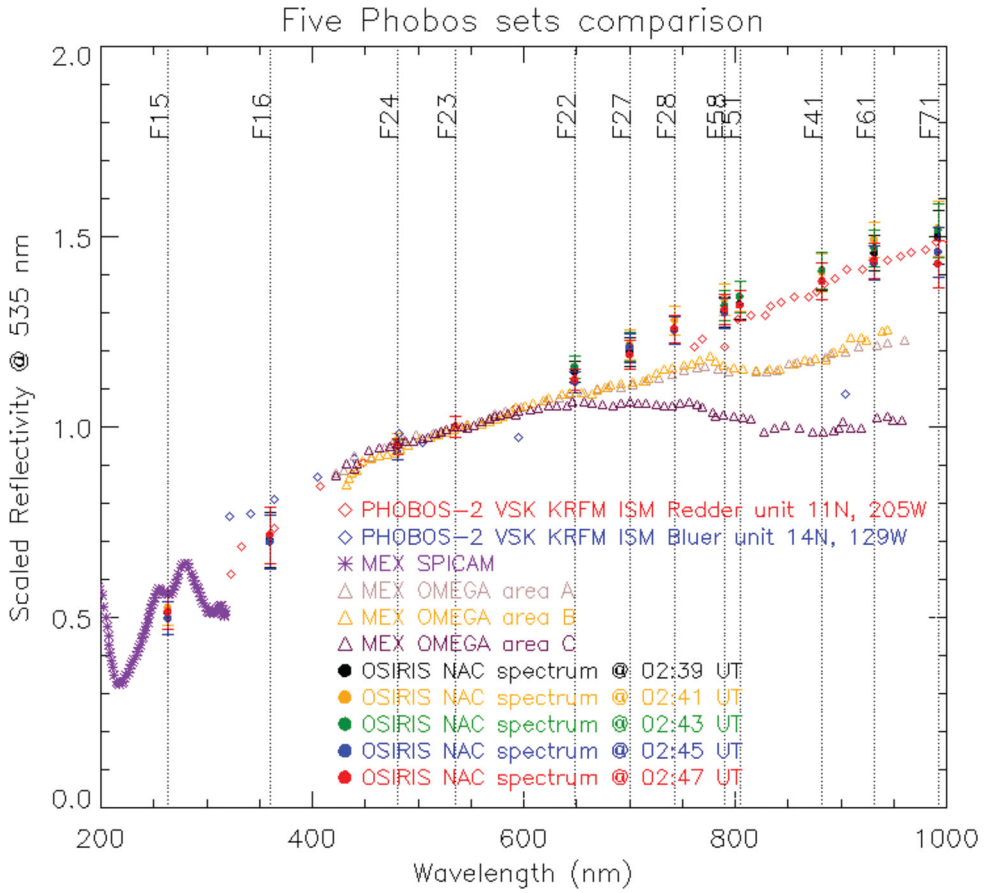


**Figure 13.** Five OSIRIS-NAC spectra obtained during the post-Mars CA phase compared with previous spectrophotometric disc-resolved observations.

because they well represent two end members and a mean type of the D-type slope range.

Our reflectance spectra are redder than the mean D-type of the Bus taxonomy, but within the reflectance of other reported D-type asteroids. In particular, it is less red than 1167 Dubiago. Our result, a set of very red spectra, suggests a composition of the surface of Phobos based on organic materials, typical of outer belt asteroids like D-type asteroids, Trojans and cometary nuclei.

We also compared our results with the Kaidun and Tagish Lake meteorites, the first one being considered a probable fragment of Phobos which has fallen on the Earth (Ivanov 2004), the latter being a D-type spectral behaviour meteorite (Hiroi, Zolensky & Pieters 2001). We then noticed that our results do not match with the Kaidun meteorite which is more similar to C-type spectral behaviour (carbonaceous chondrites), and it is more similar to the Tagish Lake spectral behaviour, even if it is slightly redder.

As reported by Kaňuchová et al. (2011), most of the surface of Phobos is characterized by red reflectance spectra, the bluer ones indicating the area close to Stickney crater. The area observed by OSIRIS is far from the Stickney crater and the high spectral slope we found in these observed areas confirms the previous findings.

### 5.2 Phobos as a captured asteroid: the dynamical model

Since our spectra support the body of data that identify Phobos as a possible outer belt D-type asteroid, we decided to explore in detail the feasibility of the capture of Phobos in the aftermath of a collision between two asteroidal bodies occurring within the sphere of influence of Mars, and to attempt to constrain the timing of such an event. In this way, we can build a robust background for interpreting the outcome of our observations.

The collisional capture scenario was first devised by Colombo & Franklin (1971) to explain the existence of families of irregular satellites of Jupiter, and it was also adopted by Turrini et al. (2009) to study the capture of irregular satellites of Saturn. In this scenario, two components contribute to the change in velocity $\delta \boldsymbol{v}$ needed to capture the parent body of Phobos. The first and dominant component is due to the conservation of the linear momentum of the two bodies and, assuming that the collision is inelastic but with a coefficient of restitution approaching 1, it is a function of the ratio of the masses of the two bodies and of their relative velocity (Turrini et al. 2009). To this component, the ejection velocities with respect to the barycentre of projectile and target must be added (Benz & Asphaug 1999).

To assess the viability of the capture of Phobos from a dynamical point of view, we calculated the possible heliocentric orbits of the putative parent body of the satellite and the conditions for its capture. Due to the time reversibility of the equations of motion, we investigate the inverse capture problem (i.e. the orbital unbinding of Phobos from Mars) taking advantage of the model and the corresponding MSSCC (Modelling Software for Satellite Collisional Capture) code developed by Turrini et al. (2009) for the capture of the irregular satellites of Saturn.

The MSSCC software employs the specific impulse $\delta \boldsymbol{v}$ needed to obtain the transition from a bound planetocentric orbit to a bound heliocentric orbit as the guiding parameter in the search for

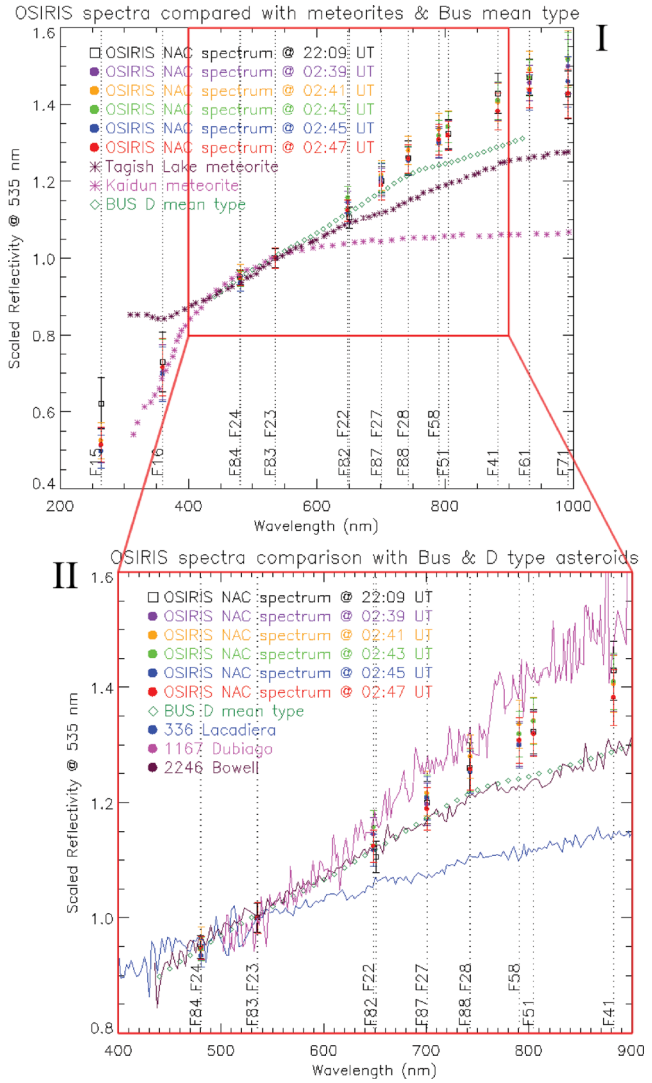


**Figure 14.** OSIRIS-NAC spectra obtained during the pre- and post-CA compared (I) with the D mean type of the Bus asteroid taxonomy, with the Kaidun and Tagish Lake meteorites and (II) with some D-type asteroids presented in Lazzarin et al. (1995) and Bus & Binzel (2002a,b). The different filters used in the pre- and post-CA are indicated.

possible pre-capture orbits. As discussed by Turrini et al. (2009), the assumption underlying the algorithm of MSSCC is that the capture of Phobos should have been due to a single, instantaneous change in velocity (i.e. a delta-shaped specific impulse).

To explore the capture of Phobos with MSSCC we used sampling steps of 5° for the $\delta \boldsymbol{v}_i$ vectors in the $x$–$y$ plane and in the $z$ direction and again 5° for the mean anomalies of Phobos and Mars: with this setup, the MSSCC code explores about $8.5 \times 10^6$ possible configurations. The mass, semimajor axis, eccentricity and inclination with respect to the ecliptic plane of Mars and the mass and inclination with respect to the ecliptic plane of Phobos have been obtained from the Horizons system of the NASA Jet Propulsion Laboratory (Giorgini et al. 1996).[2] The post-capture semimajor axis of Phobos has been assumed equal to the synchronous orbital radius of Mars ($a = 1.3656 \times 10^{-4}$ au) while the post-capture eccentricity of Phobos varied in the range 0.2–0.8.

[2] http://ssd.jpl.nasa.gov/?horizons

**Table 5.** Orbital and physical data for Mars and Phobos. The Phobos semimajor axis is indicated with respect to Mars.

| Body | Mars | Phobos |
|---|---|---|
| Mass (g) | $6.4185 \times 10^{26}$ | $1.0800 \times 10^{19}$ |
| Semimajor axis (au) | 1.5236 | $1.3656 \times 10^{-4}$ |
| Eccentricity | $9.3458 \times 10^{-2}$ | 0.2–0.8 |
| Inclination (°) | 1.8488 | 27.7200 |

The possible initial large eccentricity of Phobos, derived from the impact dynamics, would have been subsequently damped by gas drag (if the capture took place before the dissipation of the solar nebula), by the tides raised on the satellite by Mars and, to a lesser extent, by the Martian tidal torque which alone would damp an eccentricity of 0.1–0.2 over the Solar system age. In their work on the tidal evolution of the satellite, in fact, Lambeck (1979), Yoder (1982) and Burns (1986) showed that after the capture event the tidal evolution would have brought the satellite from its initial orbit, farther away from Mars but within the synchronous radius, to its present orbit on a time-scale comparable to the age of the Solar system, i.e. 4.5 Ga. It must be noted, however, that the presently observed eccentricity of Phobos is not necessarily a tidally damped remnant of an initial highly eccentric orbit. As shown by Yoder (1982), Phobos encountered three spin–orbit resonances where the eccentricity and inclination underwent significant jumps during its tidal evolution.

The physical and orbital data of Mars and Phobos used in our modelling are given in Table 5.

The results we obtain with the MSSCC software are shown in Figs 15 and 16. In Fig. 15 the different colours identify, in the [$a$–$e$] and [$a$–$i$] planes, the orbital parameters of the potential parent bodies of Phobos for different values of the $\delta \boldsymbol{v}$ required to obtain fragments in planetocentric orbits with an eccentricity of 0.2. The same colour code is used in Fig. 16 to show the orbital parameters of the potential parent bodies of Phobos required to obtain fragments in planetocentric orbits with an eccentricity of 0.8. As can be seen by the comparison of Figs 15 and 16, the main effect of the higher post-capture eccentricity is to increase by about 1 au the maximum pre-capture semimajor axis of the possible parent body of Phobos for a given value of $\delta \boldsymbol{v}$.

If we assume that the asteroids presently populating the asteroid belt did not migrate from their formation regions by more than 0.5 au throughout their histories (O'Brien, Morbidelli & Bottke 2007), the bulk of D-type asteroids should have populated the orbital region roughly comprising between 3 and 5 au. If the parent body of Phobos was indeed a D-type, in order to be captured by Mars it should have been injected on a high-eccentricity orbit and then it should have lost no less than 2 km s$^{-1}$ and more likely between 4 and 6 km s$^{-1}$ of its orbital velocity due to the collision for the capture to occur.

Such an extreme collision implies that the parent body of Phobos and the planetesimals against which it impacted had a high relative velocity. Since in the case for real, inelastic collisions the restitution coefficient is always lower than 1, a significant fraction of the linear momentum of the two bodies would be lost in the collision. As a consequence, the relative velocity between the two bodies should have been higher than the values of $\delta \boldsymbol{v}$ shown in Figs 15 and 16, which can be regarded as lower limits.

The most likely scenario to supply the high change in velocity needed is that the parent body of Phobos impacted against a planetesimal on a Mars-like orbit. This scenario and the conditions it

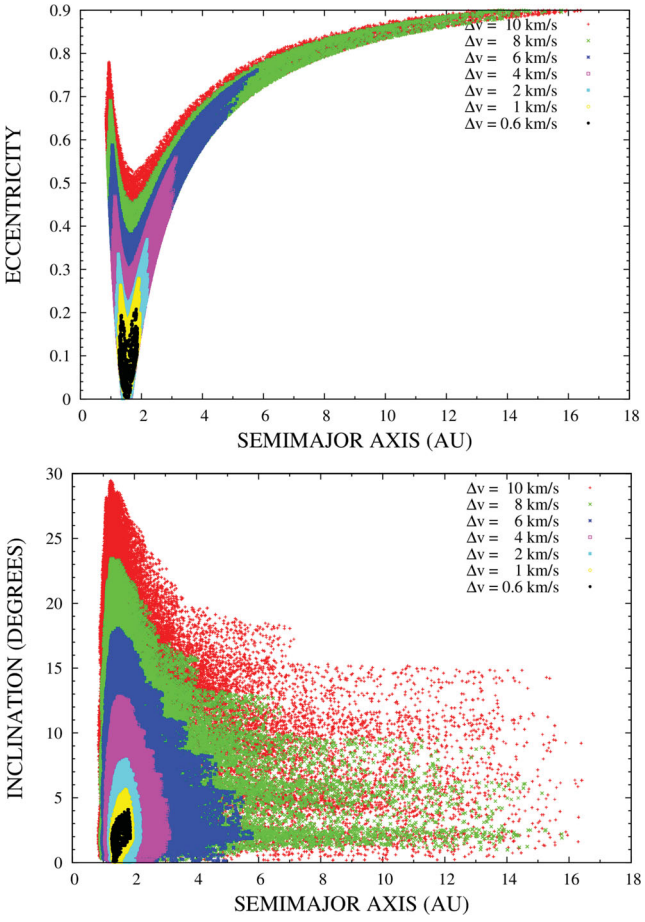


**Figure 15.** Possible heliocentric orbits of the parent body of Phobos projected in the $a$–$e$ plane (top panel) and in the $a$–$i$ plane (bottom panel). The different colours identify the value of $\delta \boldsymbol{v}$ required to capture Phobos on a primordial orbit with planetocentric semimajor axis $a = 1.3656 \times 10^{-4}$ au (i.e. the synchronous orbital radius), inclination $i = 27.^{\circ}72$ (i.e. the present-day inclination with respect to the ecliptic plane) and eccentricity $e = 0.2$.

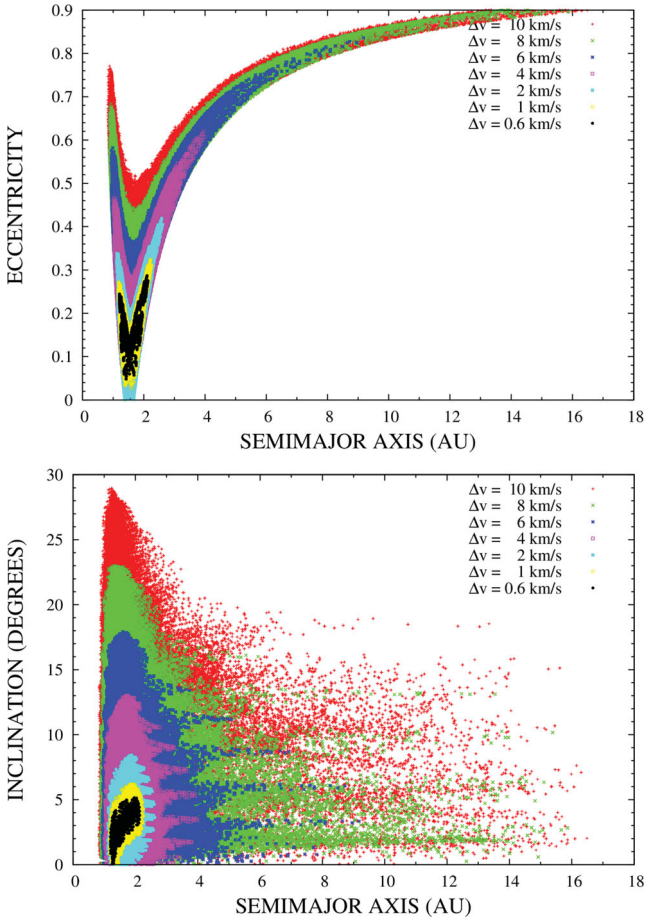


**Figure 16.** Same as Fig. 15 but for a primordial eccentricity of the captured Phobos of 0.8.

requires, however, are likely associated with a low probability of occurring. To have a realistic probability for such a capture event to occur, therefore, we need to satisfy two conditions, i.e. we need to have at the same time a large number of planetesimals in the orbital region of Mars against which the parent body of Phobos could impact, and a large flux of D-type asteroids ejected from the asteroid belt and injected into the inner Solar system on high-eccentricity orbits.

To satisfy the first condition, the capture should have taken place before or while the terrestrial planets were forming and before the dynamical depletion of the orbital region between Mars and the asteroid belt took place (Weidenschilling 1977; Wetherill 1992). This is equivalent to assuming that the capture took place during the first 100 Ma of the life of the Solar system. To satisfy the second condition, the capture should have taken place either at the time of formation of the giant planets or during the depletion of the asteroid belt. Both the latter cases are plausible since meteoritic data suggest that Mars completed its accretion in 2–6 Ma (see e.g. Dauphas & Pourmand 2011), thus likely before or contemporary with the formation of the giant planets and the dispersal of the nebular gas.

If the capture of Phobos took place at an early time when the solar nebula was still present, i.e. in less than 10 Ma after the formation of the first solids, then the flux of D-type asteroids would be related to the rapid appearance and depletion of the orbital resonances with Jupiter. This event triggered the Jovian Early Bombardment (Turrini, Magni & Coradini 2011; Turrini, Coradini & Magni 2012) and caused the injection on high-eccentricity orbits of planetesimals originally residing between 3 and 5 au which are strongly perturbed by the 2:1 resonance (at about 3.3 au) and the 3:2 resonance (at about 4 au) with the giant planet (Turrini et al. 2011).

Alternatively, the capture of Phobos could have occurred between 10 and 100 Ma after the formation of the first solids in the Solar system. In this case, the combined perturbations of planetary embryos thought to have originally resided in the asteroid belt and of both Jupiter and Saturn would have caused the ejection of a significant fraction of the planetesimals orbiting between Mars and the asteroid belt on high-eccentricity orbits, either to be accreted by the Sun or to be ejected by the Solar system (Wetherill 1992; Chambers & Wetherill 2001; Petit, Morbidelli & Chambers 2001; O'Brien et al. 2007).

Both the first and the second conditions we need to satisfy in order to have a reasonable chance to collisionally capture Phobos point towards an early capture of the satellite. After the first 10 Ma of the life of the Solar system, in fact, the population of the asteroid belt would be depleted by about one order of magnitude with respect to its original value and the inner Solar system would be devoid of

planetesimals by about the same factor (O'Brien et al. 2007). After 100 Ma, the depletion of the asteroid belt and the Martian orbital region would decrease the population of planetesimals by about another order of magnitude (O'Brien et al. 2007). As a consequence, we would lack both possible parent bodies of Phobos to inject on Mars-crossing orbits and impactors on Mars-like orbits for the collisional capture to have reasonable chances to occur.

Moreover, if the capture of Phobos took place before the dispersal of the nebular gas, the parent body of Phobos could be captured on a high-eccentricity orbit and at higher distances from Mars. The effects of the gas drag (first) and tides (after) will then shrink and circularize the orbit. If, instead, the capture took place after the dispersal of the gas, the parent body of Phobos needs to be captured on a moderately high-eccentricity orbit with semimajor axis equal to the synchronous orbital radius of Mars. As a consequence, the later the capture, the more severe are the dynamical constraints and the lower is the chance of the capture taking place.

The latter consideration holds true especially if we consider the latest possible window of opportunity for the capture of Phobos, i.e. the flux of asteroidal bodies ejected from the asteroid belt during the Late Heavy Bombardment as a consequence of the hypothesized orbital rearrangement of the giant planets in the outer Solar system (Gomes et al. 2005). While the subject of the existence and the duration of the Late Heavy Bombardment is still a matter of debate and the amount of asteroids ejected from the asteroid belt (towards both the inner and the outer Solar system) has been recently shown to be much lower than originally estimated (Minton & Malhotra 2009), in principle this event could be responsible for a late delivery of the parent body of Phobos from the outer asteroid belt to Mars.

In such a scenario, however, the number of planetesimals surviving in the Martian orbital region, if any, would be extremely low. A possible way to circumvent this problem is to assume that the capture took place following the collision of the parent body of Phobos with another asteroid ejected from the asteroid belt. If this was the case, the two asteroids needed to be on significantly different orbits (in terms of either shape or orientation in space) so that they had a high relative velocity at the time of their encounter. As we cautioned previously, however, these constraints make a late capture of Phobos far less likely than an early capture.

## 6 SUMMARY AND CONCLUSIONS

On 2007 February 24 and 25, the *Rosetta* spacecraft, en route to its main target comet 67P/Churyumov–Gerasimenko, flew by the planet Mars.

Seventy multiband images of Phobos have been taken by the OSIRIS-NAC camera in a wavelength range from 263.5 to 992.0 nm. The *Rosetta* equatorial geometry during the Mars swing-by provided unique views of Phobos.

The OSIRIS-NAC sets used for the spectrophotometric analysis of Phobos have been divided into two sections: the pre-Mars CA data obtained between 22:09:09 and 22:10:04 UT on 2007 February 24, and the post-Mars CA data obtained between 02:39:11 and 02:47.37 UT on 2007 February 25.

Due to the limited amount of pixels that sampled Phobos in the pre-CA phase and without having the possibility to discern any Phobos surface features, we decided to realize a disc-integrated spectrophotometric analysis of the Martian satellite. The area which we studied during the pre-CA with the disc-integrated aperture photometry methodology goes from 126°W to 286°W in longitude and from 90°S to 87°N in latitude, and it had already been previously studied with several different instruments onboard different spacecraft. In this work we demonstrated that all OSIRIS data fit within the errors with spectral trends of previous unresolved/disc-integrated measurements used for comparisons.

We used the same technique as for the pre-CA, with the five different data sets obtained during the post-Mars CA phase, analysing a specific area never studied at multi-wavelengths before, which goes from 0° to 43°E, entirely belonging to the sub-Mars hemisphere/redder unit. We noticed that all reflectance values for each filter in all sets agree within the errors, showing that there are no significant variations between the five different sets even if the phase angle changes from 136.°80 to 139.°61.

The reflectance plot presented shows that our data do not fit with the comparison spectra after 650 nm. This can be due to two reasons. First, the OSIRIS observed area is completely different from that of the other specific spectra. The second possible explanation of the differences between OSIRIS data and *Phobos 2* redder unit data can be the totally different observation geometry. NAC data were acquired with a phase angle which goes from 136.°80 to 139.°61, while *Phobos 2* data were obtained with a phase angle of 7.°7. The possible explanation of this difference can be due to the presence of phase reddening, a physical phenomenon which has already been previously observed on airless bodies of the Solar system.

Finally, we compared our reflectance spectra, both pre- and post-CA, with the Tagish Lake meteorite, which presents a lower spectral slope with respect to OSIRIS data, and with the spectrum of the Kaidun meteorite, which is supposed to come from Phobos, with which it does not show any match. Then we compared our data with the mean D-type spectrum of the Bus taxonomy and other D-type asteroids, obtaining that the spectra of Phobos are all redder than the mean D-type, but within the behaviour of the spectra of other D-types.

In order to put the observational results into context and verify whether the parent body of Phobos could have originally been a D-type asteroid, we used the set of data produced by OSIRIS and the current knowledge of the evolution of the early Solar system (Coradini et al. 2011) to build an updated scenario for the capture of Phobos based on the collisional mechanism first proposed for the irregular satellites of the giant planets.

We showed that D-type asteroids ejected from the asteroid belt could be captured by Mars after a collision with planetesimals in the Martian orbital region, and that such a scenario temporally locates the capture event somewhere in the first 10–100 Ma of the lifetime of the Solar system, consistently with the results of previous studies of the orbital evolution of Phobos. The earliest time when the capture can occur is that of the formation of Jupiter and of the Jovian Early Bombardment; collisional capture can occur also at later times but the likelihood of the event grows lower the more time passes due to the reduction in the flux of bodies coming from the outer regions of the Solar system.

## ACKNOWLEDGMENTS

MP thanks Dr Lucilla Rambelli and Alessandro Martignon for useful discussions regarding Phobos pre-OSIRIS observations, and Dr Gabriele Rodeghiero and Dr Riccardo Rossi for several interesting talks regarding the disc-integrated spectrophotometric analysis technique.

MP also thanks Dr Arthur Bertol and Claudia Scipioni for fruitful discussions regarding the Phobos area observed by NAC, and Dr Walter Sabolo for useful hints on the fly-by geometry of the *Rosetta*/Mars swing-by.

OSIRIS was built by a consortium led by the Max-Planck-Institut für Sonnensystemforschung, Katlenburg-Lindau, Germany, in collaboration with CISAS, University of Padova, Italy, the Laboratoire d'Astrophysique de Marseille, France, the Instituto de Astrofísica de Andalucia, CSIC, Granada, Spain, the Research and Scientific Support Department of the European Space Agency, Noordwijk, the Netherlands, the Instituto Nacional de Tecnica Aeroespacial, Madrid, Spain, the Universidad Politecnica de Madrid, Spain, the Department of Astronomy and Space Physics of Uppsala University, Sweden, and the Institut für Daten technik und Kommunikationsnetze der Technischen Universität Braunschweig, Germany.

The support of the national funding agencies of Germany (DLR), Italy (ASI), France (CNES), Spain (MEC), Sweden (SNSB) and the ESA Technical Directorate is gratefully acknowledged. We thank the *Rosetta* Science Operations Centre and the *Rosetta* Mission Operations Centre for the successful fly-by of Mars.

The authors are grateful to the anonymous referee who helped to improve the quality of the paper.

## REFERENCES

Benz W., Asphaug E., 1999, Icarus, 142, 5
Buratti B. J., Hillier J. K., Wang M., 1996, Icarus, 124, 490
Burns J. A., 1986, in Satellites. Univ. Arizona Press, Tucson, AZ, p. 117
Bus S. J., Binzel R. P., 2002a, Icarus, 158, 146
Bus S. J., Binzel R. P., 2002b, Icarus, 158, 106
Cantor B. A., Wolff M. J., Thomas P. C., James P. B., Jensen G., 1999, Icarus, 142, 414
Chambers J. E., Wetherill G. W., 2001, Meteorit. Planet. Sci., 36, 381
Clark B. E. et al., 2002, Icarus, 155, 189
Colombo G., Franklin F. A., 1971, Icarus, 15, 186
Coradini A., Turrini D., Federico C., Magni G., 2011, Space Sci. Rev., 163, 25
Dauphas N., Pourmand A., 2011, Nat, 473, 489
Domingue D. L., Robinson M., Carcich B., Joseph J., Thomas P., Clark B. E., 2002, Icarus, 155, 205
Giorgini J. D. et al., 1996, BAAS, 28, 1158
Gomes R., Levison H. F., Tsiganis K., Morbidelli A., 2005, Nat, 435, 466
Gondet B., Bibring J.-P., Langevin Y., Poulet F., Murchie S. L., 2008, in Lunar and Planetary Institute Science Conference Abstracts Vol. 39 of Lunar and Planetary Inst. Technical Report, Phobos Observations by the OMEGA/Mars Express Hyperspectral Imager. p. 1832
Gondet B., Bibring J.-P., Langevin Y., Poulet F., 2009, in European Planetary Science Congress 2009 Phobos observations by the OMEGA/Mars Express hyperspectral imager. p. 773
Gondet B., Bibring J.-P., Langevin Y., 2010, in European Planetary Science Congress 2010 Phobos observations by OMEGA/Mars Expres hyperspectral imager. p. 548
Hiroi T., Zolensky M. E., Pieters C. M., 2001, Sci, 293, 2234
Hunten D. M., 1979, Icarus, 37, 113
Ivanov A. V., 2004, Sol. Syst. Res., 38, 97
Kaňuchová Z., Baratta G. A., Brunetto R., Fulvio D., Strazzulla G., 2011, in EPSC-DPS Joint Meeting 2011, held 2–7 October 2011 in Nantes, France, Space weathering and the surface composition of Phobos, p. 148 (http://meetings.copernicus.org/epsc-dps2011)
Keller H. U., Barbieri C., Lamy P., Rickman H., 2007, Space Sci. Rev., 128, 433
Lambeck K., 1979, J. Geophys. Res., 84, 5651
Lazzarin M., Barbieri C., Barucci M. A., 1995, AJ, 110, 3058
Lederer S. M., Domingue D. L., Thomas-Osip J. E., Vilas F., Osip D. J., Leeds S. L., Jarvis K. S., 2008, Earth Planets Space, 60, 49
Lumme K., Bowell E., 1981, AJ, 86, 1694
Lynch D. K. et al., 2007, AJ, 134, 1459
Magrin S. et al., 2012, Planet. Space Sci., 66, 43
Masursky H., Batson R. M., Carr M. H., McCauley J. F., 1972, in Bulletin of the American Astronomical Society Vol. 4 of Bulletin of the American Astronomical Society, Mariner 9 Mars Television Experiment. p. 356
Minton D. A., Malhotra R., 2009, Nat, 457, 1109
Murchie S., 1999, J. Geophys. Res., 104, 9069
Murchie S., Erard S., 1996, Icarus, 123, 63
Murchie S. et al., 2007, in Exploration of Phobos and Deimos MRO/CRISM Observations of Phobos and Deimos. p. 27
Murchie S. L. et al., 2008, in Lunar and Planetary Institute Science Conference Abstracts Vol. 39 of Lunar and Planetary Inst. Technical Report, MRO/CRISM Observations of Phobos and Deimos. p. 1434
O'Brien D. P., Morbidelli A., Bottke W. F., 2007, Icarus, 191, 434
Pang K. D., Rhoads J. W., Lane A. L., Ajello J. M., 1980, Nat, 283, 277
Perrier S., Stern A. S., Bertaux J. L., 2004, in AAS/Division for Planetary Sciences Meeting Abstracts #36 Vol. 36 of Bulletin of the American Astronomical Society, Spatially Resolved UV albedo spectra of PHOBOS with SPICAM on Mars Express. p. 1137
Petit J.-M., Morbidelli A., Chambers J., 2001, Icarus, 153, 338
Pollack J. B., Veverka J., Pang K. D., Colburn D. S., Lane A. L., Ajello J. M., 1978, Sci, 199, 66
Rivkin A. S., Brown R. H., Trilling D. E., Bell J. F., Plassmann J. H., 2002, Icarus, 156, 64
Rosenblatt P., 2011, A&AR, 19, 44
Schröder S. E., Lüthi B., Gunderson K., 2009, in European Planetary Science Congress 2009 Rosetta's OSIRIS Observes Steins Phase Reddening. p. 461
Thomas N., Britt D. T., Herkenhoff K. E., Murchie S. L., Semenov B., Keller H. U., Smith P. H., 1999, J. Geophys. Res., 104, 9055
Turrini D., Marzari F., Tosi F., 2009, MNRAS, 392, 455
Turrini D., Magni G., Coradini A., 2011, MNRAS, 413, 2439
Turrini D., Coradini A., Magni G., 2012, ApJ, 750, 8
Warell J., Bergfors C., 2008, Planet. Space Sci., 56, 1939
Weidenschilling S. J., 1977, Ap&SS, 51, 153
Wetherill G. W., 1992, Icarus, 100, 307
Yoder C. F., 1982, Icarus, 49, 327
Zellner B., Wells E. N., 1994, in Lunar and Planetary Institute Science Conference Abstracts Vol. 25 of Lunar and Planetary Inst. Technical Report, Spectrophotometry of Martian Satellites with the Hubble Space Telescope. p. 1541

This paper has been typeset from a TEX/LATEX file prepared by the author.